Numerical simulation of pollutant dispersion in the atmosphere based on 3D Navier-Stokes equations

Tyatyushkina E.S.[1,2], Kozelkov A.S. [1,2], Giniyatullin R.R. [4], Shishlenin M.A.[3], and Strelets D.Yu.[2]

[1)] Nizhny Novgorod State Technical University, Nizhny Novgorod.
[2)] Moscow Aviation Institute, Moscow.
[3)] Sobolev Institute of Mathematics, Novosibirsk.
[4)] Independent researcher.

In the present paper, numerical 3D simulation of pollutant dispersion in the atmosphere is described based on the solution of a complete system of fluid dynamics equations, i.e. Reynolds-averaged Navier-Stokes equations supplemented with concentration transport equations under the Fick's diffusion law. The proposed mathematical model makes it possible to accurately simulate gaseous pollutant transport disregarding the empirical regularities. The advantages of this approach include the ability to make adjustments for turbulence, terrain, wind rose data, underlying surface, pollution source geometry, compressibility of the medium, and accurate atmospheric stratification settings. In the paper, we present the numerical simulation results for point-source propane emission and dispersion of mixed emission from a chimney with calculation of the maximum near-ground pollutant concentration. The simulation results are validated by comparison to the experimental data and by calculating maximum instantaneous concentrations of emissions from a single point source.
It is shown that the proposed approach ensures the desirable measurement accuracy for all hydrodynamic parameters of polluted air dispersion.

The results have been obtained with the backing of the Science and Universities National Project under the Russian Ministry of Education and Science grant for the development of new young researcher labs no. FSWE-2024-0001 (Research subject: Development of numerical methods, models, and algorithms to describe fluid and gas flows under natural conditions and in presence of industrial facilities operating under normal and emergency conditions using exascale and zettascale computing), and the Establishment and Development Program for the World-Class Research Center 'Supersonic' for 2020-2025 supported by the Russian Ministry of Education and Science (Project no. 075-15-2022-309 dated April 20, 2022). The work by M.A. Shishlenin was supported by RSCF project 24-41-04004 «Identification and research of mathematical models in science and industry - regularization and machine learning».

Keywords: numerical simulation, Navier-Stokes equations, turbulence, pollutants, near-ground concentration, pollution source, air pollution

Introduction

Air pollution is a major issue of today's world, as it poses a direct health and environmental threat. This problem has become increasingly relevant in recent years due to industrial growth. Air pollution occurs as a result of daily emissions from industrial facilities, motor vehicles and aircraft, as well as municipal waste incineration. It is linked to major health risks, such as incidence of pulmonary, cardiovascular, and other diseases, which in turn causes an increase in healthcare expenses [World Health Organization, 2021]. On top of that, air pollution contributes to global climate change [European Commission, 2010; Pantusheva et al., 2022].

The process of pollutant distribution and dispersion in the natural atmosphere is affected by a number of factors, such as atmospheric stability; site location and terrain; height and size of industrial buildings and structures; location and geometric dimensions of sources (for example, mouth diameter and chimney height); temperature and density of emission; pollutant state, etc. [Aloyan, 2002]. In addition, pollutant dispersion in the atmosphere depends on meteorological

factors, such as wind speed and direction; presence and type of inversions; temperature stratification; air humidity; atmospheric pressure; wind calmness, precipitation, fogs, etc.

There are reference values of maximum permissible concentrations for stationary and mobile pollution sources, which are further specified for particular models of motor vehicles. The hazard level of the near-ground atmospheric air pollution with emissions from industrial facilities is determined based on the highest calculated value of near-ground pollutant concentration. In most cases, the latter is calculated using the empirical formulas described in [Atmosphere. Reference manual, 1991].

In addition to statistical and in-situ measurements, as well as empirical analytical algorithms, we can analyze some other pollutant dispersion calculation methods. Thanks to the significant advances in computing technology, pollution concentration evaluation using numerical algorithms has become a promising research area [Zhang, et al., 2020; Glazunov, 2018; Baker et al., 2004]. In particular, it is worth mentioning computational fluid dynamics methods, which are considered the most consistent and accurate and are also widely used in geophysical simulations [Kozelkov et al., 2023]. A complete system of fluid dynamics equations, i.e. Navier-Stokes equations supplemented with heat transfer equations, taking into account the multicomponent nature of emissions makes it possible to rather accurately simulate the gaseous pollutant transport disregarding the empirical regularities. Another advantage of the approach is high simulation accuracy achieved by making adjustments for flow turbulence [Kozelkov et al., 2022], terrain (underlying surface) [Kozelkov et al., 2023] and geometry of pollution sources, compressibility, and accurate density dependence on temperature. The calculation results show the highest level of detail, because all the calculated parameters are represented at each point of the modeled area, which makes it possible to extract more data from the calculations and make more detailed predictions.

A review of methods simulation gaseous pollutant dispersion in the atmosphere has been carried out [Antonova et al., 2019], and Pasquill's method based on the Gaussian model turned out to be preferable for calculations having to do with dispersion of gaseous pollutants produced by power generating installations under various atmospheric condition categories assuming constant meteorological factors [Asadi et al., 2017]. Software complex SKAT may be used to predict near-ground pollutant concentrations and carry out atmospheric pollutant dispersion calculations for the purpose of monitoring pollutant emissions in presence of operational industrial facilities.

In [Andersen et al., 2024], the authors described Danish Lagrangian Model (DALM), a new high-resolution air pollution model based on the concept of Lagrangian particles. Theoretical fundamentals of the model were presented, and validation of DALM was described against measurements applying different combinations of the implemented parameterizations, which

demonstrated that DALM could accurately reproduce spatiotemporal patterns in the measured data and that its performance was more sensitive to parameterizations of vertical compared to horizontal transport.

In [Raheja et al., 2021], a 2-phase simulation model was presented to assess air quality to evaluate toxicity level of each pollutant in the air, which can harm the health of sensitive people. A comparison was presented for the air quality index under the 2-phase assessment model with the air quality indices presented by Indian government agencies. It was shown that the proposed model could be used to assess the air quality in urban areas.

In [Zhang et al., 2022], the hourly data obtained from air quality monitoring stations in China in 2016 were used to calculate the annual mean and annual standard deviation of six air quality indicators at each station based on Self-Organizing Maps (SOM) and K-mean clustering algorithms.

In [Egorkin et al., 2023], HYSPLIT model was used in the simulation to determine the area of negative impact sources, and the emission transport from the supposed negative impact sources to the Crimea region was analyzed. In addition, the sensitivity of simulation was studied for inverse and direct trajectories of air mass transfer.

There is a series of papers dedicated to pollutant dispersion simulation using RANS approach. In [Silva et al., 2023], the authors presented a study of pollutant dispersion in the air using OpenFOAM-based simulation of fluid dynamics. It was shown that aerodynamic effects were more important at lower wind speeds, as they reduced turbulent dispersion of pollutants and allowed for a more significant reduction of pollutant concentrations in the air. In [Huang et al., 2021], the effect of wind speed and direction on pollutant dispersion in the air as a result of roadside emissions was studied taking into account the seasonal cycles in Tejgaon and Gazipur, two of the main districts in the Bangladeshi city of Dhaka. In [Sedlyarov & Borodina, 2022], the simulation of pollutant dispersion in the near-ground atmospheric layer as a result of acetone emission from an isolated source located in close proximity of a building was performed taking into account the terrain and development pattern using computational fluid dynamics, specifically the RANS approach. In [Danilkin & Starchenko, 2020; Starchenko et al., 2022; Danilkin & Starchenko, 2020; Danilkin et al., 2023], the authors presented the results of RANS simulation of non-isothermal turbulent air flow and impurity transport as a result of motor vehicle emissions in an idealized street canyon. The evaluated effect of the street canyon size [Danilkin & Starchenko, 2020; Starchenko et al., 2022, Dai et al., 2020; Chen et al.,2021; Lobaccaro et al., 2019; Huang et al.,2021] and the degree of surface heating [Starchenko et al., 2022] on the average pollutant concentration in the breathing zone. In [Weerasuriya et al., 2022], simulation of a mixed emission from a point source in the form of a short chimney is studied taking into account the chemical reactions

involved. In [Zhang K. et al., 2020; Zhang Y. et al., 2020a, 2020b], a series of RANS simulations was performed to investigate the reactive pollutant dispersion in 3D street canyons taking into account the effects of uneven solar heating of building surfaces, governed flow fields in deep and shallow street canyons, as well as urban areas with various building densities and heights. Apart from the RANS approach, the papers are also available, where pollutant dispersion in urban canyons is simulated using LES approach [Glazunov, 2018; Baker, 2004; Xie & Castro, 2009; Zhong et al., 2017; Kikumoto&Ooka, 2018; Woodward et al., 2019; Zhou et al., 2021] and direct numerical simulation (DNS) [Rossi, 2010; Goulart, 2018]. These papers are indicative of the current development of computational methods for pollutant dispersion problems. There is still a number of problems requiring further study, such as calibration of the utilized models against the available experimental data or in-situ observations; development of a unified CFD simulation methodology for the discussed type of simulation problems; investigation of numerical scheme dissipation; adjusting for the terrain; introduction of additional models to make adjustments for wind rose data and Coriolis force.

A brief review on the mathematical simulation of air pollutant dispersion in the atmosphere was provided in [Leelőssy et al., 2014] along with advantages and shortcomings of various simulation strategies, namely Gaussian, Lagrangian, Eulerian, and CFD models.

In [Reiminger et al., 2023], CFD was used to evaluate the effect of road designs with the road's surface lower than the surrounding ground level on the downwind pollutant concentrations for eight road depths and thirteen stability conditions (Richardson numbers). Depressed roads can decrease downwind pollutant concentrations compared to classical roads, but only under neutral and unstable temperature conditions. Four equations making it possible to predict downwind pollutant concentrations depending on the distance from the road centerline, the road depth, and thermal stability. The results of the study may inform pre-construction recommendations on whether a depressed road should be considered to protect human health, as well as provide predictive tools to assess the beneficial or adverse impact of such structures on air quality.

In [Sukhinov et al., 2011, 2015], mathematical simulation of impurity dispersion in the air medium was carried out for coastal regions. A new mathematical model of aerodynamic processes taking into account a variety of factors relevant for coastal zones, as well as heat and mass transfer processes in the air medium of coastal zones, intended for mapping of turbulent flows for the velocity field of a multicomponent air medium on high-resolution meshes was proposed for the calculation of pollutant concentrations.

In this paper, we present the results of numerical simulation of pollutant dispersion based on Reynolds-averaged 3D Navier-Stokes equations supplemented with concentration transport equations [Landau&Lifshitz, 1988; Loytsyansky, 1973]. Numerical method is based on the finite

volume method on arbitrary unstructured meshes created by the automatic mesh generator [Borisenko et al., 2018, 2022]. This approach makes it possible to automatically make adjustments for the underlying surface terrain and as a general matter solve geophysical problems (including pollutant dispersion) for random natural areas [Kozelkov et al., 2023]. To evaluate the accuracy of the method, we performed numerical simulation for two problems as follows: simulation of propane emission from a single source with determination of pollutant mass fraction along the jet trajectory and simulation of mixed emission dispersion from a single chimney with determination of the maximum near-ground pollutant concentration taking into account the wind conditions. The calculation results are compared against the experimental data for the first problem and the theoretical solution for the second problem. The results of the numerical simulation performed demonstrate the viability of computational fluid dynamics methods for solving this types of problems. The numerical method presented in the paper provides a solution for a forward problem of pollutant dispersion, which can be used to state an inverse problem of determining the maximum permissible pollutant concentration at the point. This inverse problem is reduced to determining the distance to the pollution source based on the concentration level at the given point, or, in other words, with the data on near-ground pollutant concentrations available, it is possible to reconstruct the emission source data.

Mathematical model

To simulate pollutant (concentration) dispersion, we can use the system of Reynolds-averaged Navier-Stokes equations supplemented with concentration transport equations under the Fick's diffusion law written down as follows [Landau&Lifshitz, 1988; Ferziger&Peric, 2002]:

$$\begin{cases} \dfrac{\partial \rho}{\partial t} + \dfrac{\partial}{\partial x_i}\left(\rho u_i\right) = 0, \\ \rho \dfrac{\partial u_i}{\partial t} + \rho \dfrac{\partial}{\partial x_j}\left(u_i u_j\right) = -\dfrac{\partial p}{\partial x_i} + \dfrac{\partial}{\partial x_j}\left(\tau_{ij} + \tau^t{}_{ij}\right) + \rho g_i, \\ C_p \dfrac{\partial \rho T}{\partial t} + \dfrac{\partial}{\partial x_i}\left(\rho u_i T\right) = -\dfrac{\partial}{\partial x_i}\left(\lambda \Delta T\right) + \dfrac{\partial}{\partial x_i}\left(u_i\left(\tau_{ij} + \tau^t{}_{ij}\right)\right) + \dfrac{\partial \rho}{\partial t} + S_T \\ \dfrac{\partial \rho c_k}{\partial t} + \dfrac{\partial}{\partial x_i}\left(\rho u_i c_k + q_{c_k}\right) = S_{c_k}, k = 1...n-1 \end{cases}, \quad (1)$$

where i and j are subscripts indicating that vector components belong to Cartesian coordinates, $i, j = \{x, y, z\}$; ρ is the medium density, u_i is the velocity vector component, $i = \{x, y, z\}$; t is the time; p is the pressure; x_i is the vector component in Cartesian coordinates, $i = \{x, y, z\}$; T is the temperature; μ is the molecular viscosity; C_p is the specific heat capacity; λ is the effective

thermal conductivity coefficient of the medium; τ_{ij} is the viscous stress tensor, which, according to the Boussinesq's hypothesis, is written down as follows:

$$\tau_{ij} = \mu\left(\frac{\partial u_i}{\partial x_j} + \frac{\partial u_j}{\partial x_i} - \frac{2}{3}\frac{\partial u_k}{\partial x_k}\delta_{ij}\right),$$

μ is the dynamic viscosity; δ_{ij} is the Kronecker delta; g_i is the gravitational acceleration vector component.

To calculate component concentrations, we analyze their volume fractions:

$$c_k, 0 \le c_k \le 1, \sum_{k=1}^{n} c_k = 1.$$

The final component is calculated explicitly using the concentration of the other components as follows:

$$c_k = 1 - \sum_{k=1}^{n-1} c_k.$$

Diffusion flow of the c_k component is derived using the diffusion coefficient under the Fick's law:

$$\vec{q}_{C_l} = -D_k c_k, k = 1...n-1$$

where D_k is the component's diffusion coefficient. Diffusion flow can also be derived by setting the Schmidt number: $\vec{q}_{C_l} = -\frac{\mu}{S_C}\nabla c_k$.

When the turbulent case is considered, we should also take into account the turbulent component of the concentration diffusion flow:

$$\vec{q}_{c_l} = -\left(\frac{\mu}{S_C} + \frac{\mu_t}{S_{Ct}}\right)\nabla c_k \ ,$$

where μ_t is the turbulent viscosity.

To solve the problems of pollutant dispersion in the atmosphere, the Navier-Stokes system of equations is enriched with possible sources of energy S_T and concentrations S_{C_k}. This approach makes it possible to take into account both point-type and finite-radius mobile sources. It is also possible to introduce a group of sources of different nature. In this case, the respective sources in the right part of the discretized equations are summed up.

System of equations (1) is incomplete due to unknown relationship between a pivotal variable τ_{ij}^t and averaged flow parameters. This relationship reflecting the contribution of turbulent flow pulsations to the main flow may be clarified using additional relationships generally referred to as turbulence models [Menter et al., 2003; Kozelkov et al., 2022].

To make turbulence simulation possible, the system (1.2.5) should be enriched with additional relationships. In the present paper, we use SST, one of the better-known RANS turbulence models presented in its classical form in [Menter et al., 2003]. SST model is a differential turbulence model, which uses empirical relationships for the turbulent viscosity coefficient μ_t, while Boussinesq's hypothesis and Fourier's law are used for stress tensor calculation as follows:

$$\tau^t_{ij} = 2\mu_t\left(S_{ij} - \frac{1}{3}I_{ij}\nabla\cdot\vec{u}\right) + \frac{2}{3}kI_{ij},\ S_{ij} = \frac{1}{2}\left(\frac{\partial u_i}{\partial x_j} + \frac{\partial u_j}{\partial x_i}\right).$$

In RANS SST turbulence model, $k-\varepsilon$ model is stated in $k-\omega$ terms and intended for small-scale turbulence resolution in the outer part of the flow, while $k-\omega$ model intended for describing large-scale turbulence is used in the boundary layer. These two models are combined using the F_1 function ensuring the proximity of the combined model to the $k-\varepsilon$ model at a distance from solid walls and to the $k-\omega$ model in the near-wall part of the flow:

$$\begin{aligned}
&\frac{\partial\rho k}{\partial t} + \frac{\partial}{\partial x_j}\left(\rho u_j k\right) = \frac{\partial}{\partial x_j}\left[\left(\mu + \sigma_k\mu_T\right)\frac{\partial k}{\partial x_j}\right] + P_k - \beta^*\rho\omega k,\\
&\frac{\partial\rho\omega}{\partial t} + \frac{\partial}{\partial x_j}\left(\rho u_j \omega\right) = \frac{\partial}{\partial x_j}\left[\left(\mu + \sigma_k\mu_T\right)\frac{\partial\omega}{\partial x_j}\right] + \gamma\frac{\rho}{\mu_T}P_k - \beta\rho\omega^2 + \left(1-F_1\right)D_{k\omega},
\end{aligned} \tag{2}$$

where $\omega = \varepsilon/k$ is the specific kinetic energy dissipation rate.

The generation term in transport equations (2) is calculated as follows:

$$P_k = \min\left(\mu_T S^2, 20\beta^*\rho k\omega\right),\ \ S^2 = 2S_{ij}S_{ij}, \tag{3}$$

with the rightmost term in the right part of the transport equation ω is derived as follows:

$$D_{k\omega} = \frac{2\rho\sigma_{\omega 2}}{\omega}\frac{\partial k}{\partial x_i}\frac{\partial\omega}{\partial x_i}. \tag{4}$$

Rather than using the standard relationship $\mu_T = k/\omega$ to determine the turbulent viscosity with k and ω available, the SST model uses a different expression based on the well-known Bradshaw assumption as follows:

$$\mu_T = \frac{a_1 k}{\max(a_1\omega, \Omega F_2)}, \tag{5}$$

which limits the viscosity in the near-wall region and allows us to avoid the separation delay typical for $k-\varepsilon$ models. The empirical function F_2 in (5) is calculated as follows:

$$F_2 = \tanh(\arg_2^2), \tag{6}$$

where $\arg_2 = \max\left(\frac{2\sqrt{k}}{0.09\omega d_w}, \frac{500\nu}{d_w^2\omega}\right)$, and d_w is the distance to the closest point of a solid surface.

Empirical constants of the model are determined based on the respective constants from $k-\varepsilon$ and $k-\omega$ models using the aforementioned F_1 function:

$$\begin{aligned} \sigma_k &= F_1\sigma_{k1} + (1-F_1)\sigma_{k2}, \\ \sigma_\omega &= F_1\sigma_{\omega 1} + (1-F_1)\sigma_{\omega 2},, \\ \beta &= F_1\beta_1 + (1-F_1)\beta_2, \end{aligned} \tag{7}$$

$$F_1 = \tanh(\arg_1^4), \arg_1 = \min\left[\max\left(\frac{\sqrt{k}}{0.09\omega d_w}, \frac{500\nu}{d_w^2\omega}\right), \frac{4\rho\sigma_{\omega 2}k}{CD_{k\omega}d_w^2}\right], \tag{8}$$

$$CD_{k\omega} = \max\left\{D_{k\omega}, 10^{-20}\right\}.$$

Here, subscripts 1 and 2 in (7) are attributed to the constants of $k-\omega$ and $k-\varepsilon$ models respectively:

$$\begin{aligned} &\sigma_{k1} = 0.85,\ \sigma_{\omega 1} = 0.5, \quad \beta_1 = 0.075, \\ &\sigma_{k2} = 1.0,\ \ \sigma_{\omega 2} = 0.856,\ \beta_2 = 0.0828, \\ &\beta^* = 0.09,\ k = 0.41,\ a_1 = 0.31,\ \gamma = \beta/\beta^* - \sigma_\omega k^2/\sqrt{\beta^*}. \end{aligned} \tag{9}$$

In the present paper, this model is used in combination with the universal near-wall functions [Grotjans & Menter, 1998; Menter et al., 2003] ensuring a satisfying accuracy of the solution with an arbitrary mesh resolution within the boundary layer.

System of equations (1) is discretized using the finite volume method on an arbitrary unstructured mesh, and its numerical resolution is achieved using the fully implicit method [Chen&Przekwas, 2010; Kozelkov et al., 2018] based on the well-known SIMPLE algorithm. To simulate free surface flows, SIMPLE algorithm should be modified in a specific way. The detailed description of the main formulas for the modified SIMPLE algorithm, the boundary conditions, and the implementation may be found in [Chen&Przekwas, 2010; Kozelkov et al., 2018; Moukalled&Darwish, 2004].

Here we present the finite-volume discretization scheme for the main equations used in the paper. Scalar transport equation, which is the basic equation for solving system (1), is written down as follows:

$$\frac{\partial\rho\varphi}{\partial t} + \frac{\partial}{\partial x_j}\left(\rho\varphi u_j\right) = \frac{\partial}{\partial x_j}\tau_j + Q. \tag{10}$$

The first term in (10) is a non-stationary term, the second one a convective term, and then a diffusion term. The equation may also include sources and sinks represented by the rightmost term Q. Tensor τ_j includes spatial derivatives of the desired value φ.

For the simplicity sake, we assume $\tau_j = \mu \frac{\partial \varphi}{\partial x_j}$. It makes the calculations much less cumbersome without reducing the generality of the methods described below.

Here, we consider an arbitrary unstructured mesh as presented in Fig. 1:

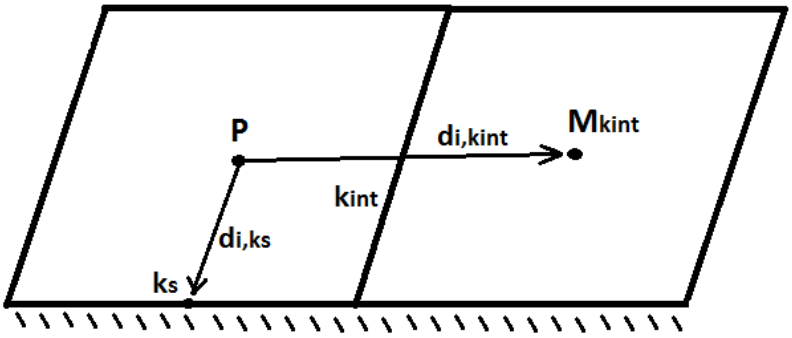

Fig. 1. Computational mesh (*k* is the multitude of faces for the cell *P* consisting of a set of internal faces k_{int} and a set of external faces k_s).

The neighbor cell sharing the same internal face k_{int} will be referred to as $M_{k_{int}}$ and vector area of the face k as $S_{i,k}$, where i = 0..2 is the vector component number. The vector drawn from the center of cell P towards the center of cell M through the face k_{int} will be referred to as $d_{i,k_{int}} = r_{i,M} - r_{i,P}$, and the one drawn from the center of P towards the center of the face as $d_{k_s} = r_{k_s} - r_P$, where r_i is the radius vector.

Discretization of (10) with respect to time using the second-order scheme, namely the Adams-Bashforth scheme [Roache, 1980], is as follows:

$$\frac{3\rho^{j+1}\varphi^{j+1} - 4\rho^{j}\varphi^{j} + \rho^{j-1}\varphi^{j-1}}{2\Delta t} + \left[\frac{\partial}{\partial x_j}\left(\rho\varphi u_j\right) - \frac{\partial}{\partial x_j}\tau_{ij} - Q \right]^{j+1} = 0. \qquad (11)$$

To perform spatial discretization of (10) we integrate it with respect to the P cell volume and then integrate convection and diffusion terms with respect to the area:

$$\int_{V_P} \frac{3\rho^{j+1}\varphi^{j+1} - 4\rho^{j}\varphi^{j} + \rho^{j-1}\varphi^{j-1}}{2\Delta t} dV + \oiint_{S_P} \rho\varphi u_j dS_j - \oiint_{S_P} \mu \frac{\partial \varphi}{\partial x_j} dS_j - \int_{V_P} Q dV = 0. \qquad (12)$$

Discretization of the source and the nonstationary term is carried out as follows:

$$\int_{V_P} \frac{\rho^{j+1}\varphi^{j+1} - \rho^{j}\varphi^{j}}{\Delta t} dV = \left(\frac{\rho^{j+1}\varphi^{j+1} - \rho^{j}\varphi^{j}}{\Delta t} \right)_P V_P, \int_{V_P} Q dV = Q_P V_P. \qquad (13)$$

A discrete analogue of the diffusion term is written down as follows [Roache, 1980]:

$$\oiint_{S_P} \mu \frac{\partial \varphi}{\partial x_j} dS_j \approx \sum_k \left(\mu \frac{\partial \varphi}{\partial x_j} \right)_k S_{j,k} = \sum_k \mu_k \left(\frac{\partial \varphi}{\partial n_k} \right)_k |S_k|, \qquad (14)$$

where n_k is the normal line to the face k. A derivative with respect to direction $\frac{\partial \varphi}{\partial n_k}$ occurring in the product behind the summation sign in the right part of the equation may be determined as follows in the case of orthogonal computational mesh:

$$\frac{\partial \varphi}{\partial n_k}|S_k| = \frac{\varphi_M - \varphi_P}{|d_k|}|S_k|. \quad (15)$$

For the purposes of approximation on a finite volume mesh, convective term is written down as follows:

$$\oint_{S_P} \rho \varphi u_j dS_j \approx \sum_k \rho_k \varphi_k u_{j,k} S_{j,k} \approx \sum_k \rho_k \varphi_k F_k , \quad (16)$$

where F_k is the volumetric flow through the face k. The value at the face φ_k is determined by the discretization scheme used for the convective term. There are numerous discretization schemes applicable on arbitrary unstructured meshes [Jasak, 1996; Jasak et al, 1999; Leonard, 1979; Gaskell, 1988]. Among those, we can identify a few having the highest applicability ratings, such as Upwind Differences (UD), Linear Upwind Differences (LUD), QUICK, Central Differences (CD), NVD (Normalized Variable Diagram) family of differencing schemes, and hybrid schemes (the aforementioned schemes combined with the upwind scheme to increase monotonicity). Each scheme has a peculiar way of reconstructing the desired values at the face and, as a result, its own unique dissipative properties [Kozelkov et al., 2014].

By using the aforementioned discretization, we replace (10) with the system of linear algebraic equations (SLAE) written down for each cell of the computational mesh:

$$A_P \varphi_P + \sum_{k_{int}} A_{k_{int}} \varphi_{M_{k_{int}}} = R_{i,P} . \quad (17)$$

This SLAE is solved using an iterative solver. For instance, LOGOS software suite uses a multigrid AMG solver for all SLAEs [Volkov et al., 2014].

Theoretical calculation method for maximum instantaneous concentrations from single point source emissions

In most cases, the near-ground pollutant concentration (C_{max}) is calculated in practice using the empirical formulas described in [Atmosphere. Reference manual, 1991]. Typically, C_{max} is determined at a certain distance from the emission site under the most adverse meteorological conditions. The near-ground concentration is defined as a concentration measured at the bottom two meter thick air layer. The maximum near-ground concentration C_{max} for the emission of a heated gas-air mixture from a single source with a circular mouth is determined as follows [Atmosphere. Reference manual, 1991]:

$$C_{max} = \frac{A \cdot M \cdot F \cdot m \cdot n \cdot \eta}{H^2 \cdot \sqrt[3]{V_i \cdot \Delta T}} \quad (18)$$

where H is the height of the emission source above the ground level, m; ΔT is the temperature difference between the emitted gas-air mixture and the surrounding air temperature; M is the amount of pollutants emitted into the atmosphere (g/s); A is the coefficient depending on temperature stratification, which is different for each region [Atmosphere. Reference manual, 1991]; F is the dimensionless coefficient taking into account pollutant deposition rate in the atmosphere [Atmosphere. Reference manual, 1991]; $V_i = \frac{\pi D^2}{4} W$ is the consumption of the gas-air mixture; D is the mouth diameter of the emission source; W is the average exit rate of the gas-air mixture at the mouth of the emission source, m/s; m, n are the coefficients taking into account the exit conditions of the gas-air mixture at the mouth of the emission source; η is the coefficient taking into account the terrain ($\eta = 1$ for flat and slightly uneven terrains).

Coefficient m is calculated depending on the value f [m/(s2·°C)] as follows:

$$m = \begin{cases} \frac{1}{0.67 + 0.1\sqrt{f} + 0.34\sqrt[3]{f}}, f < 100 \\ \frac{1.47}{\sqrt[3]{f}}, f \geq 100. \end{cases}, \text{ where } f = 10^3 \frac{W^2 D}{H^2 \Delta T}.$$

The emissions with $f \geq 100$ are considered cold, and the ones with $f < 100$ heated.

The value of f_e for cold emissions is calculated as $f_e = 800\left(V_m^{'}\right)^3$.

The dimensionless coefficient n is calculated depending on the value V_m as follows:

$$n = \begin{cases} 1, V_m \geq 2 \\ 0.53V_m^2 - 2.13V_m + 3.13, 0.5 \leq V_m < 2. \\ 4.4V_m, V_m < 5 \end{cases}$$

Coefficient n for cold emissions is calculated similarly to the one for heated emissions at $V_m = V_m^{'}$.

The value V_m for heated emissions is calculated as

$$V_m = 0.65\sqrt[3]{\frac{V_i \cdot \Delta T}{H}},$$

and for cold emissions as

$$V_m = 1.3\frac{WD}{H}.$$

The distance X_{max} (m) from the emission sources, where the near-ground concentration C (mg/m^3) under adverse meteorological conditions reaches its maximum C_{max} is calculated as follows:

$$X_{max} = \frac{5-F}{4} dH.$$

Dimensionless coefficient d depends on the coefficient f and is calculated as follows:

- for heated emissions ($f < 100$):

$$d = \begin{cases} 2.48\left(1+0.28\sqrt[3]{f_e}\right), V_m \le 0.54 \\ 4.95V_m\left(1+0.28\sqrt[3]{f_e}\right), 0.5 < V_m \le 2, \\ 7\sqrt{V_m}\left(1+0.28\sqrt[3]{f_e}\right), V_m > 2 \end{cases}$$

- for cold emissions ($f \ge 100$):

$$d = \begin{cases} 5.7, V_m' \le 0.5 \\ 11.4V_m', 0.5 < V_m' \le 2. \\ 16\sqrt{V_m'}, V_m' > 2 \end{cases}$$

Near-ground pollutant concentrations C in the atmosphere along the plume axis at various distances from the emission source are calculated as follows:

$$C = S_1 \cdot C_{max}. \qquad (19)$$

Dimensionless coefficient S_1 depends on the relationship $\frac{x}{x_{max}}$ and is calculated as follows:

at $\frac{x}{x_{max}} \le 1$ $\qquad S_1 = 3\left(\frac{x}{x_{max}}\right)^4 - 8\left(\frac{x}{x_{max}}\right)^3 + \left(\frac{x}{x_{max}}\right)^2,$

at $1 < \frac{x}{x_{max}} \le 8$ $\quad S_1 = \frac{1.13}{0.13\left(\frac{x}{x_{max}}\right)^2 + 1},$

at $\frac{x}{x_{max}} > 8, F = 1$ $\quad S_1 = \frac{\frac{x}{x_{max}}}{3.58\left(\frac{x}{x_{max}}\right)^2 - 3.52\frac{x}{x_{max}} + 120},$

at $\frac{x}{x_{max}} > 8, F = 2; 2.5; 3$ $\quad S_1 = \frac{1}{0.1\left(\frac{x}{x_{max}}\right)^2 + 2.47\frac{x}{x_{max}} - 17.8}.$

Equations (18)-(19) will be used below to evaluate near-ground pollutant concentrations for single chimney emissions of industrial facilities.

Numerical experiments

Numerical simulation of propane emission from a single source

The simulation of propane emission from a circular chimney into the atmospheric air (oxygen-nitrogen mixture) was chosen for the verification of the described numerical method [Strahle&Lekoudis, 1985; Schefer&Dibble, 1985]. Here, we evaluated the dispersion of the propane mass fraction at a distance from the chimney along the jet trajectory. A simplified presentation of the problem is shown in Fig. 2. The chimney has an outer diameter of 11 mm and inner diameter of 5.2 mm. The air flow speed is 9.2 m/s, and the propane emission rate is 53 m/s.

The density of the propane-air mixture is calculated as follows:

$$\rho = \frac{P_{op}}{RT\sum_{i'}\frac{m_{i'}}{M_{i'}}},$$

where R is the universal gas constant, $m_{i'}$ is the mass fraction of component i', $M_{i'}$ is the molecular weight of component i', P_{op} is the operating pressure considered equal to the atmospheric pressure.

Viscosity of the propane-air mixture is $1.72 \cdot 10^{-5}$ kg/(m·s), temperature of propane and the surrounding air is 300 K, and turbulent Schmidt number is 0.7. The initial air flow in the area consists of two components, namely oxygen (O_2) and nitrogen (N_2). The initial mass fraction of oxygen is 0.23 and nitrogen 0.77. The chimney emission consists fully of propane (mass fraction of 1).

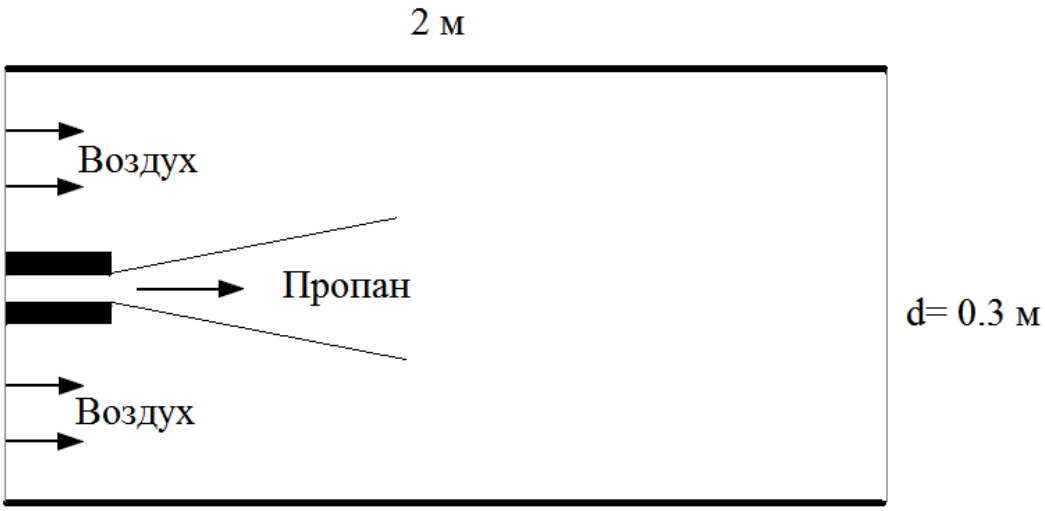

Fig. 2 – Visual presentation of the problem

Воздух –> Air

Пропан –> Propane

м –> m

For the purposes of numerical simulation, a mesh model including 115 thousand cells was designed. The mesh has a condensation at the pollutant exit and along the jet trajectory. Due to axisymmetric nature of the problem, the geometry was simplified to a sector shape.

The distribution of propane mass fraction along the plume axis is shown in Fig. 3 and the obtained velocity field in Fig. 4.

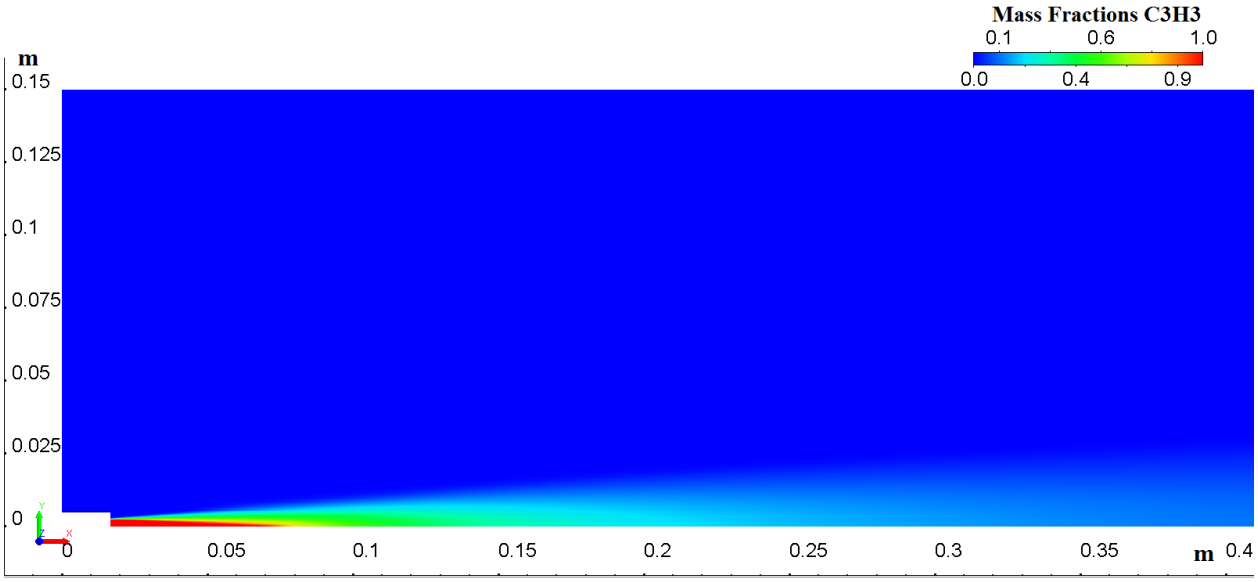

Fig. 3 – Distribution of propane mass fraction along the plume axis

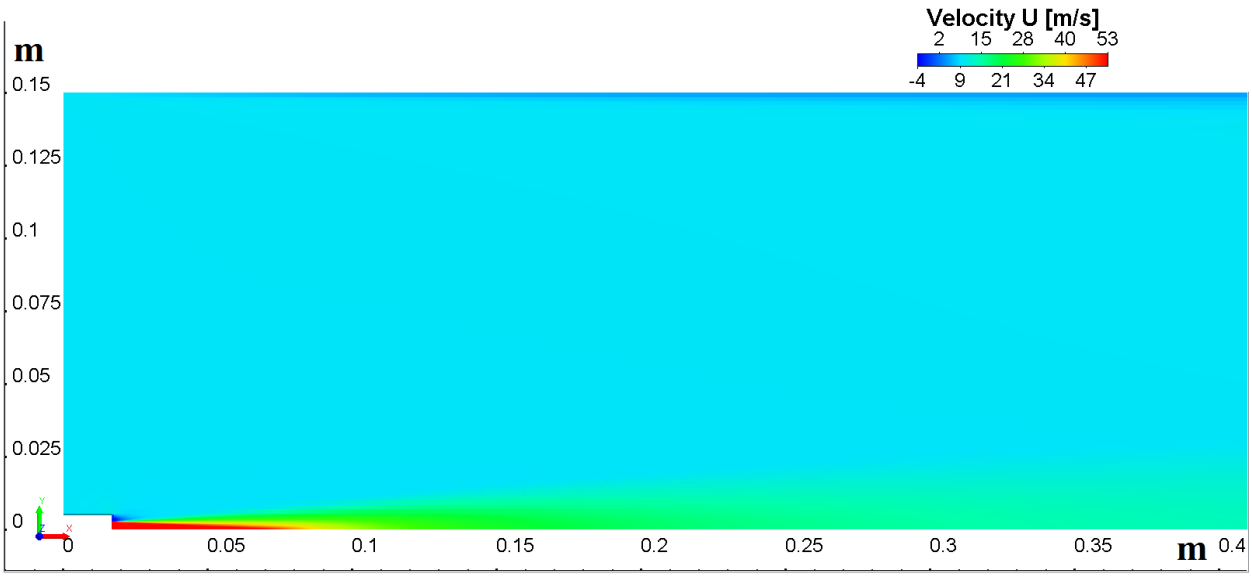

Fig. 4 – Velocity field

The experimental dataset for the distribution of propane mass fraction along the jet trajectory is available for this problem [Strahle& Lekoudis, 1985; Schefer& Dibble, 1985]. The plot showing the calculated distribution of propane mass fraction compared to the experiment is shown in Fig. 5.

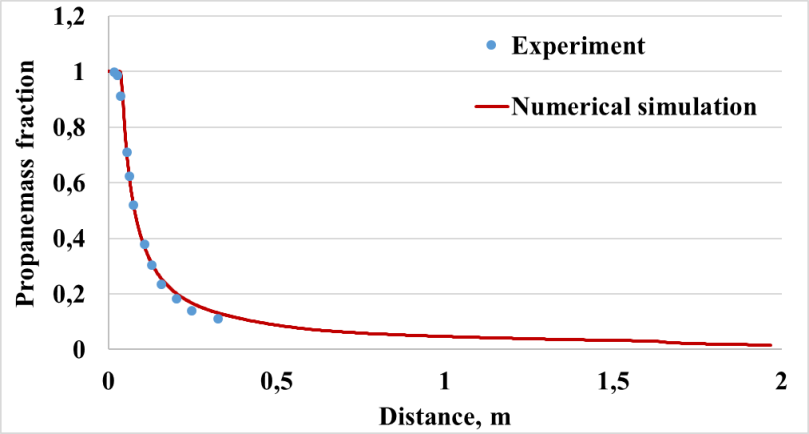

Fig. 5 – Distribution of propane mass fraction along the plume axis compared to the experiment

It can be seen from the presented plots and diagrams that propane mass fraction changes follow nearly a hyperbolic law. The maximum propane concentration is detected at the source exit. It then starts decreasing and closely approaches zero at a distance of two meters from the source. The plot shows that the numerical simulation results agree well with the experimental data. It is also worth mentioning that the simulation results allow us to evaluate the pollutant concentration at any point of the calculation area with the desired accuracy.

Numerical simulation of mixed emission dispersion from a single chimney

Here, numerical simulation of pollutant dispersion from a single chimney is performed and near-ground pollutant concentrations are determined. The visual presentation of the problem is shown in Fig. 6.

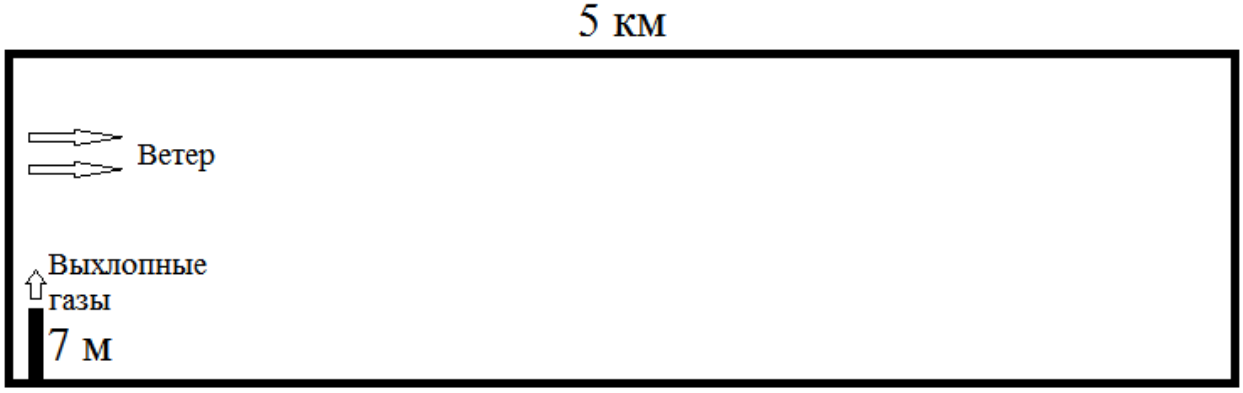

Fig. 6 – Visual presentation of the problem

км –> km

Ветер –> Wind

Выхлопные газы –> Exhaust gas

м –> m

The chimney has a rectangular mouth of 0.5 m in length and 0.4 m in width. The emitted gas temperature is $T_г = 75^o C$, the average exit rate of the air-gas mixture is $W = 14 м/с$, the surrounding air temperature is $T_в = 21.4^o C$, and wind speed is 14 m/s. The pollutant concentrations emitted into the atmosphere are as follows: $C(CO) = 3.63 г/м^3$; $C(NO_2) = 0.085 г/м^3$; $C(SO_2) = 0.38 г/м^3$; $C(NH_3) = 0.2 г/м^3$.

When we solve this problem by calculating the maximum instantaneous concentrations assuming single point source emissions [Atmosphere. Reference manual, 1991] and using coefficient values $A = 160$ (according to the temperature stratification for the European part of the Russian Federation and the Urals region to the north from 52°N), $F = 1$ (for gaseous pollutants (sulfur dioxide, carbon disulfide, etc.) and fine aerosols (dust, ash etc.) having a near-zero deposition rate), we obtain the maximum near-ground pollutant concentration C_{max} using the equation (18) as follows: $C_{max}(CO) = 2.42 мг/м^3$; $C_{max}(NO_2) = 0.057 мг/м^3$; $C_{max}(SO_2) = 0.253 мг/м^3$; $C_{max}(NH_3) = 0.133 мг/м^3$.

The near-ground concentration values *C* obtained using equation (19) for CO at distances of 250, 500, 1500, 3000, and 5000 m are presented in Table 1.

Table 1 – Pollutant concentrations at various distances from the source

Distance from the source, m	CO concentration, mg/m3	NO_2 concentration, mg/m^3	SO_2 concentration, mg/m^3	NH_3 concentration, mg/m^3
250	0.63	0.015	0.066	0.034
500	1.66	0.039	0.174	0.092
1500	2.12	0.050	0.220	0.117
3000	1.26	0.030	0.132	0.070
5000	0.64	0.015	0.067	0.035

Numerical simulation was performed using the 3D computational mesh primarily consisting of regular hexahedra. The total number of cells of the computational mesh was 15.5 M. A fragment of the computational mesh cross-section in close proximity of the chimney is presented in Fig. 7. The mesh has a condensation at the exit of exhaust gas from the chimney and at their dispersion area.

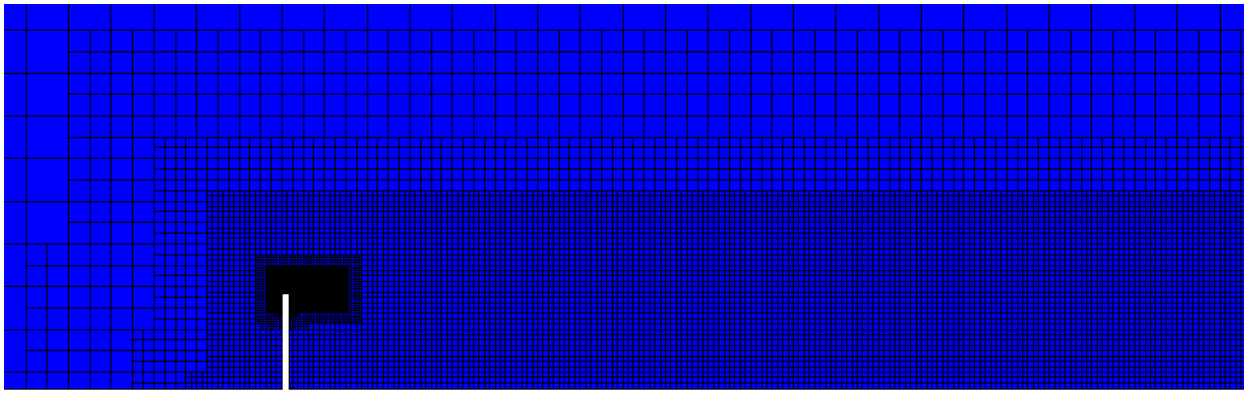

Fig. 7 – Computational mesh cross-section

The numerical simulation results showing the pollutant concentration dispersion pattern for CO, as well as temperature and velocity distributions are shown in Figs. 8–10. Concentration dispersion fields for NO_2, SO_2, and NH_3 have similar distribution patterns with varying quantitative characteristics.

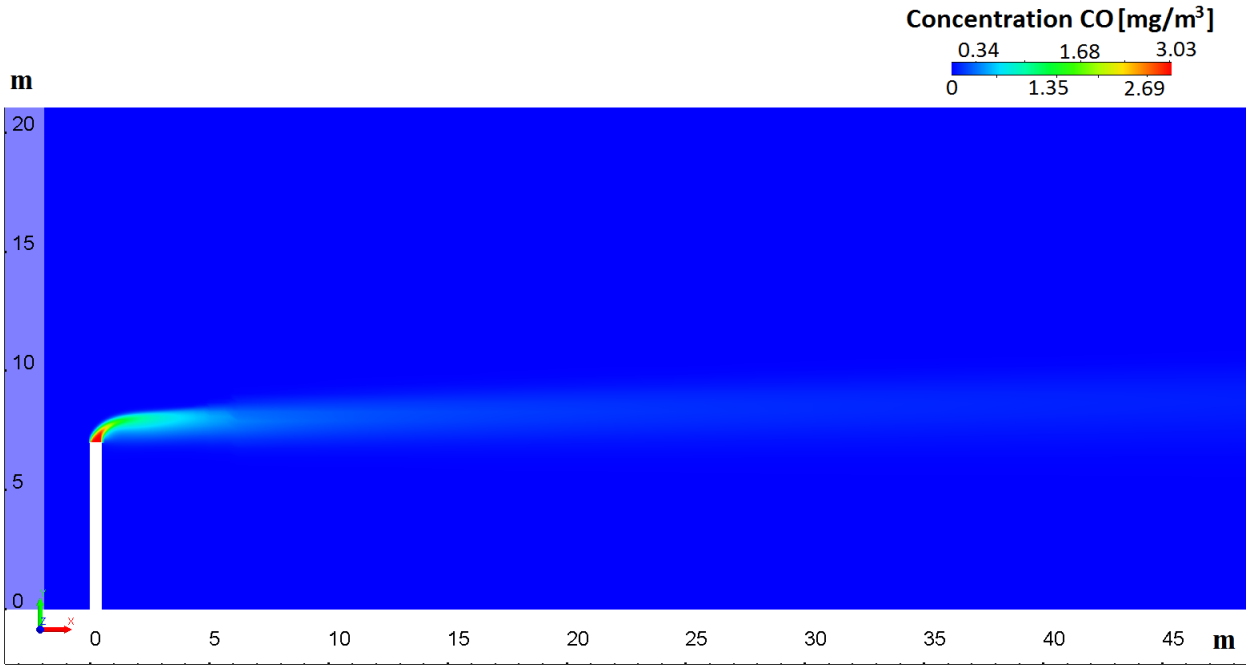

Fig. 8 – *CO* concentration dispersion field in close proximity of the chimney

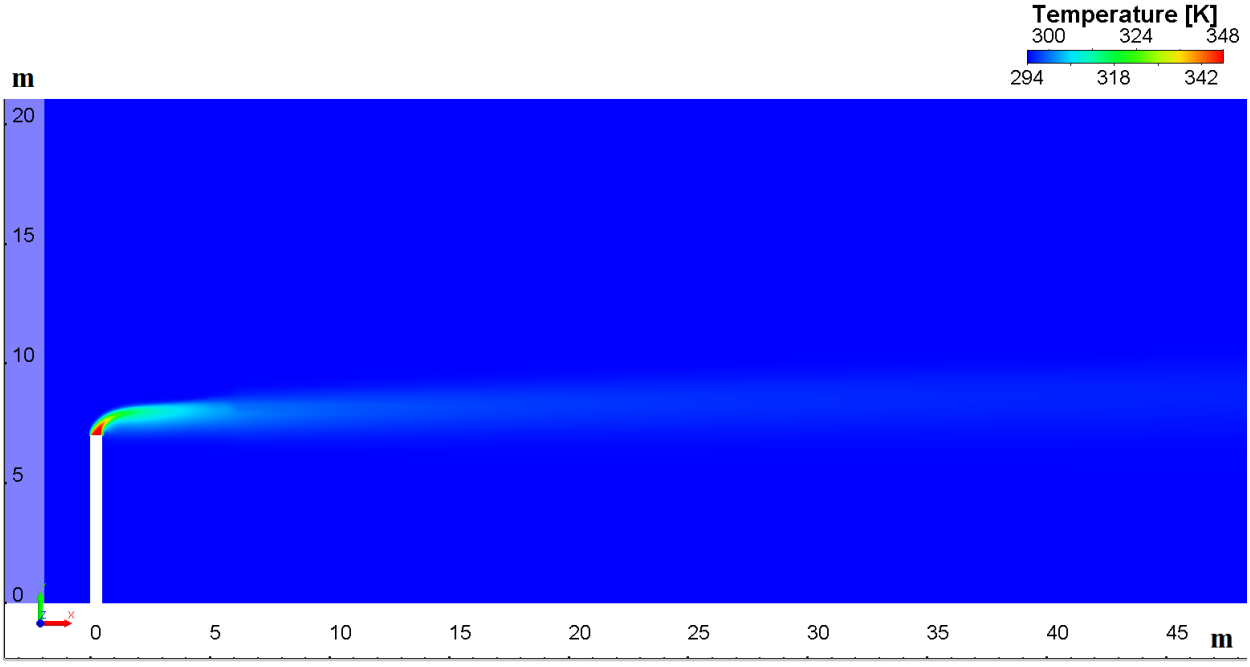

Fig. 9 – Temperature distribution field in close proximity of the chimney

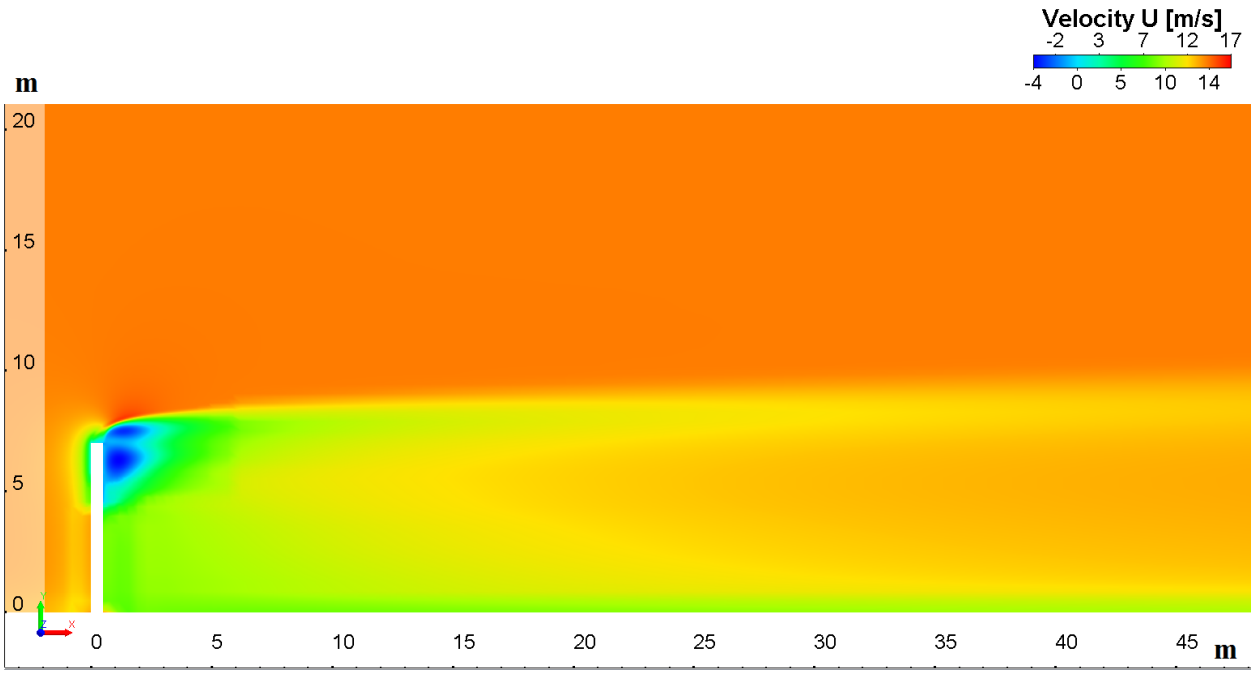

Fig. 10 – Velocity distribution field in close proximity of the chimney

To give a visually clearer representation of pollutant concentration dispersion, we present the CO dispersion pattern at the distances of up to 5000 m from the source (Fig. 11). The maximum near-ground CO concentration is observed at distances of 1000-1500 m from the source, and then it gradually decreases. The changes in the near-ground pollutant concentration depending on the distance from the source are shown in the plots in Fig. 12.

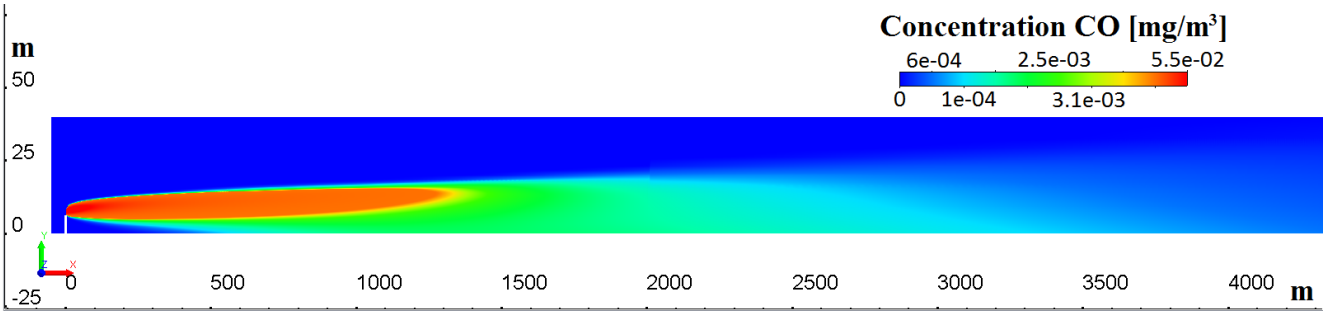

Fig. 11 – CO concentration dispersion field far from the source

The comparison of near-ground pollutant concentrations for CO, NO_2, SO_2, and NH_3 obtained by numerical simulation and the ones calculated based on maximum instantaneous concentrations assuming a single point source emission, i.e. the theoretical data, is shown in Fig. 12.

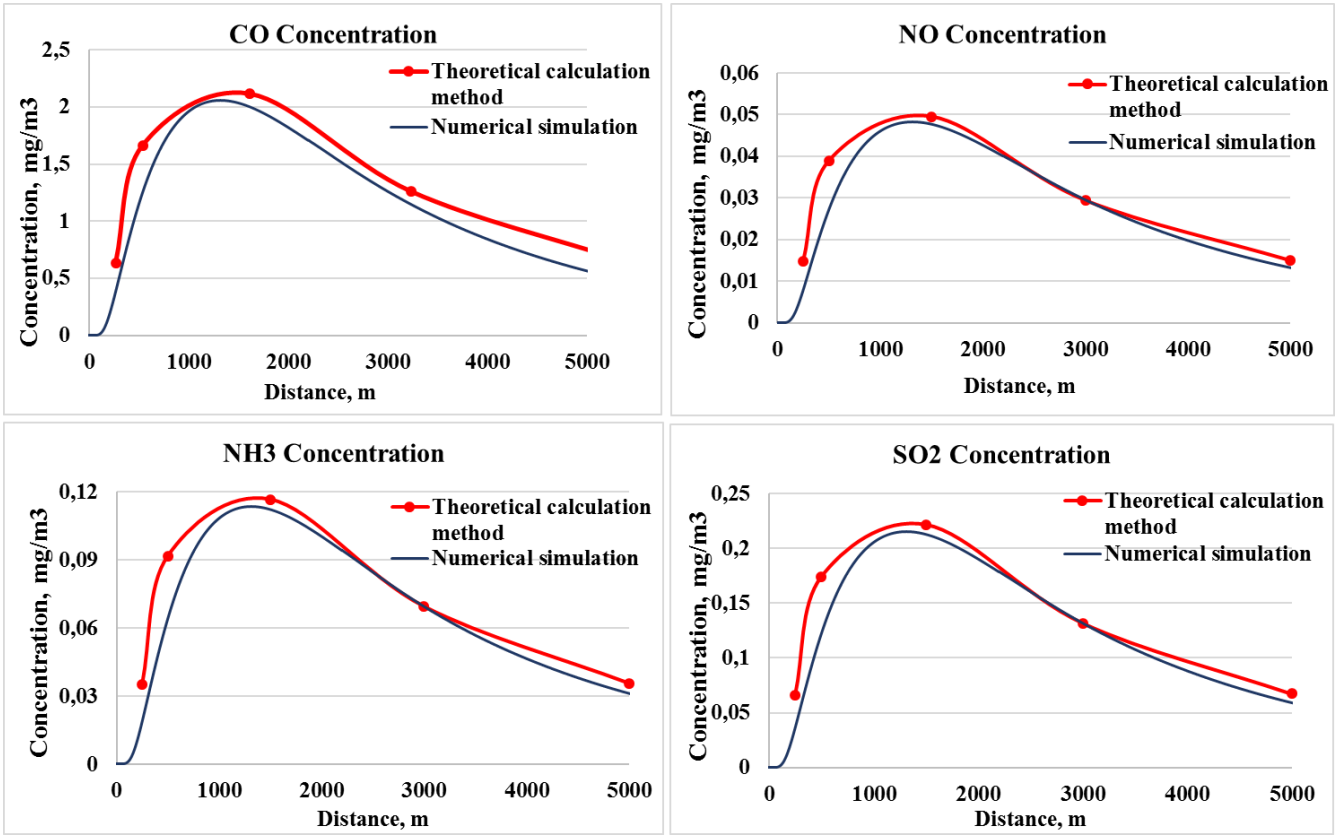

Fig. 12 – Comparison of numerical simulation results with theoretical derivations

We can see from the plots that the near-ground pollutant concentration dispersion obtained by numerical simulation agrees rather well with theoretical derivations. We can also see a good qualitative agreement between the results at various distances from the emission source, and a near matching position of the maximum concentration from the source. However there is still a certain noticeable quantitative difference between the results. This difference can possibly be caused by a mismatch (error) in determination of near-ground concentrations in the theoretical approach, since equations (18)-(19) used for concentration calculation are derived using a series of assumptions and empirical coefficients.

Conclusions

In the present paper, the numerical simulation results for pollutant dispersion in the atmospheric air have been presented with the validation examples as follows: propane emission from a single source with determination of pollutant mass fraction along the jet trajectory compared to the experimental data and mixed emission dispersion from a single chimney of an industrial facility with determination of the maximum near-ground pollutant concentration compared to the theoretical calculation of the maximum permissible emission. The simulation was carried out using the Russian engineering analysis software suite LOGOS. Numerical simulation method was based on solving the averaged Navier-Stokes system of equations supplemented with

concentration transport equations under the Fick's diffusion law. This method ensures a rather accurate simulation of gaseous pollutant transport disregarding the empirical regularities. The method also makes it possible to carry out numerical simulation taking into account the flow turbulence, the terrain, and the pollutant source geometry. The results obtained show that the applied numerical simulation method adequately describes pollutant dispersion in the atmospheric air. In the future work, it is planned to solve the inverse problem of determining the right hand side of the equation and determine the localization of pollution sources and the power of pollution.

References

1. Ali, M.E.; Hasan, M.F.; Siddiqa, S.; Molla, M.M.; Nasrin Akhter, M. FVM-RANS Modeling of Air Pollutants Dispersion and Traffic Emission in Dhaka City on a Suburb Scale. Sustainability 2023, 15, 673.
2. Andersen Ch., Ketzel M., Hertel O., Christensen J. H., Brandt J.. The Danish Lagrangian Model (DALM): Development of a new local-scale high-resolution air pollution model. Environmental Modelling & Software. 2024. Volume 176, 106010.
3. Asadi M., Asadollahfardi G. , Fakhraee H. , Mirmohammadi M.. The comparison of Lagrangian and Gaussian models in predicting of air pollution emission using experimental study, a case study: Ammonia emission. Environmental Modeling & Assessment. 2017. V. 22. P. 27–36.
4. Baker J., Walker H.L., Cai X. A study of the dispersion and transport of reactive pollutants in and above street canyons - a large eddy simulation, Atmos. Environ. 38 (39) (2004) 6883–6892, https://doi.org/10.1016/j.atmosenv.2004.08.051.
5. Chen L., Hang J., Chen G., Liu S., Lin Y., Mattsson M., Sandberg M., Ling H.. Numerical investigations of wind and thermal environment in 2D scaled street canyons with various aspect ratios and solar wall heating. Building and Environment, 2021, v.189, p.107510.
6. Chen Z.J., Przekwas A.J., A coupled pressure-based computational method for incompressible/compressible flows // Journal of Computational Physics, 2010, v. 229, p.9150-9165.
7. Dai Y., Mak C.M., Zhang Y., Cui D., Hang J.. Investigation of interunit dispersion in 2D street canyons: A scaled outdoor experiment. Building & Env., 2020, v.171, p.106673.
8. Danilkin E.A., Starchenko A.V.. Modeling the spread of automobile emissions in a street canyon // Computational technologies, 2020, v.25, №2, p.4-21.
9. Egorkin A. A., Voskresenskaya E. N., Zhuravskiy V. Y. Simulation of Pollutants Trajectory in the Black Sea Region Atmosphere with Different Spatial Resolution. Preprints 2023, 2023111695. https://doi.org/10.20944/preprints202311.1695.v1
10. European Commission. Air Pollution and Climate Change. Science for Environmental Policy. 2010. Available online: https://environment.ec.europa.eu/research-and-innovation/science-environment-policy_en (accessed on 5 August 2024).
11. Ferziger J.H., Peric M. Computational Method for Fluid Dynamics. Springer-Verlag, New York, 2002.

12. Gaskell P.H. Curvature-compensated convective-transport - SMART, A new boundedness-preserving transport algorithm. // Int. J. Numer.Methods Fluids, 1988, vol. 8, p. 617-641.
13. Glazunov A.V. Numerical simulation of turbulence and transport of fine particulate impurities instreet canyons. Numerical Methods and Programming. 2018; 19(1):17–37. (In Russ.) https://doi.org/10.26089/NumMet.v19r103
14. Goulart E.V., Coceal O., Belcher S.E. Dispersion of a passive scalar within and above an urban street network, Boundary-Layer Meteorol. 166 (3) (Mar. 2018) 351–366, https://doi.org/10.1007/s10546-017-0315-5.
15. Grotjans, H., and Menter, F.R., Wall functions for industrial applications. In K.D. Papailiou, Editor, Computational Fluid Dynamics'98, 1998, Volume 1, Part 2, p. 1112-1117, Chichester. ECCOMAS, John Wiley Sons.
16. Huang Y., Lei C., Liu C.H., Perez P., Forehead H., Kong S., Zhou J.L.. A review of strategies for mitigating roadside air pollution in urban street canyons. Environmental Pollution, 2021, v.280, p.116971
17. Jasak H. Error Analysis and Estimation for the finite volume method with applications to fluid flows. Thesis submitted for the degree of doctor // Department of Mechanical Engineering, Imperial College of Science, 1996.
18. Jasak H., Weller H.G., Gosman A.D. High resolution NVD differencing scheme for arbitrarily unstructured meshes // International journal for numerical methods in fluids, 1999, vol. 31, p. 431-449.
19. Kikumoto H., Ooka R. Large-eddy simulation of pollutant dispersion in a cavity at fine grid resolutions, Build. Environ. 127 (Jan. 2018) 127–137, https://doi.org/ 10.1016/j.buildenv.2017.11.005.
20. Kozelkov A. S., Lashkin S. V., Efremov V.R., Volkov K. N., Tsibereva Yu.A., Tarasova N.V. An implicit algorithm of solving Navier–Stokes equations to simulate flows in anisotropic porous media // Computers and Fluids. 2018. V. 160. P. 164-174.
21. Kozelkov A., Kurulin V., Emelyanov V., Tyatyushkina E., Volkov K. Comparison of convective flux discretization schemes in detached-eddy simulation of turbulent flows on unstructured meshes // Journal of Scientific Computing, 2016, v. 67, p. 176-191.
22. Kozelkov A., Tyatyushkina E., Kurkin A., Kurulin V., Kurkina O., Kochetkova O., Fluid flow simulation in a T-connection of square pipes using modern approaches to turbulence modeling // Siberian Electronic Mathematical Reports, 2022, p.144-164, http://semr.math.nsc.ru.
23. Kozelkov A.S., Bogomolov L.M., Smaznov V.V., Kurulin V.V., Tyatyushkina E.S. Simulation of landslide tsunami in the Russian Far East based on 3D Navier–Stokes equations

// Fundamental and Applied Hydrophysics, 2023, v. 16(3), p.30-51, doi:10.59887/2073-6673.2023.16(3)-3.

24. Kozelkov A.S., Krutyakova O.L., Kurulin V.V., Strelets D.Yu., Shishlenin M.A., The accuracy of numerical simulation of the acoustic wave propagations in a liquid medium based on Navier-Stokes equations // Siberian Electronic Mathematical Reports. 18(2), p. 1238-1250. 2021. http://semr.math.nsc.ru.
25. Leelőssy A., Molnár F., Izsák F., Havasi A., Lagzi I. and Mészáros R. Dispersion modeling of air pollutants in the atmosphere: a review. Open Geosciences, vol. 6, no. 3, 2014, pp. 257-278.
26. Leonard B.P. A stable and accurate convective modeling procedure based on quadratic upstream interpolation // Comput. Methods Appl.Mech/Eng., 1979, vol.19, pp. 59-98.
27. Lobaccaro G., Acero J.A., Martinez G.S., Padro A., Laburu T., Fernandez G.. Effects of Orientations, Aspect Ratios, Pavement Materials and Vegetation Elements on Thermal Stress inside Typical Urban Canyons. International Journal of Environmental Research and Public Health, 2019, v.16, p.3574
28. Menter, F. R., Kuntz, M., and Langtry, R., Ten Years of Industrial Experience with the SST Turbulence Model // Turbulence, Heat and Mass Transfer 4, ed: K. Hanjalic, Y.Nagano, and M. Tummers, Begell House, Inc., 2003, p. 625 – 632.
29. Moukalled F., Darwish M. Pressure-Based Algorithms for Multi-Fluid Flow at All Speeds-Part I: Mass Conservation Formulation, Numerical Heat Transfer, Part B: Fundamentals, 2004, v. 45, p. 495-522.
30. Pantusheva, M.; Mitkov, R.; Hristov, P.O.; Petrova-Antonova, D. Air Pollution Dispersion Modelling in Urban Environment Using CFD: A Systematic Review. Atmosphere 2022, 13, 1640. https://doi.org/10.3390/atmos13101640.
31. Raheja S., Obaidat M. S., Sadoun B., Malik S., Rani A., Kumar M., Stephan Th.. Modeling and simulation of urban air quality with a 2-phase assessment technique. Simulation Modelling Practice and Theory. 2021. Volume 109, 2021, 102281.
32. Reiminger N., Jurado X., Maurer L., Vazquez J., Wemmert C. Influence of depressed road configuration on downwind pollutant concentrations: A CFD study under various thermal stability conditions. Journal of Wind Engineering and Industrial Aerodynamics 2023. Volume 235. 105361.
33. Rossi R., Philips D.A., Iaccarino G. A numerical study of scalar dispersion downstream of a wall-mounted cube using direct simulations and algebraic flux models, Int. J. Heat Fluid Flow 31 (5) (Oct. 2010) 805–819, https://doi.org/10.1016/j.ijheatfluidflow.2010.05.006.

34. Schefer R.W., Dibble R.W., Simultaneous Measurements of Velocity and Density in a Turbulent Nonpremixed Flame, AIAA Journal, 23:1070–1078, 1985.
35. Silva V. A., Zaze E. G., Bastos P. A., Devecchi F. P., & Kolicheski M. B. (2023). Urban Pollutant Dispersion on a Turbulent Fluid Model. Trends in Computational and Applied Mathematics, 24(4), 617–633.
36. Strahle W.C., Lekoudis S.G. Evaluation of Data on Simple Turbulent Reacting Flows, AFOSR TR-85 0880, Chapter 2, School of Aerospace Engineering, Georgia Institute of Technology, Atlanta, GA. 1985.
37. Weerasuriya A.U., Zhang Xuelin, Tse K.T., Liu Chun-Ho, Kwok Kenny C.S. RANS simulation of near-field dispersion of reactive air pollutants, Building and Environment 207 (2022). https://doi.org/10.1016/j.buildenv.2021.108553
38. Woodward H., Stettler M., Pavlidis D., Aristodemou E., ApSimon H., Pain C. A large eddy simulation of the dispersion of traffic emissions by moving vehicles at an intersection, Atmos. Environ. 215 (Oct. 2019) 116891, https://doi.org/10.1016/j.atmosenv.2019.116891.
39. World Health Organization. WHO Global Air Quality Guidelines: Particulate Matter (PM2.5 and PM10), Ozone, Nitrogen Dioxide, Sulfur Dioxide and Carbon Monoxide; World Health Organization: Geneva, Switzerland, 2021; p. 12.
40. Xie Z.-T., Castro I.P. Large-eddy simulation for flow and dispersion in urban streets, Atmos. Environ. 43 (13) (Apr. 2009) 2174–2185, https://doi.org/10.1016/ j.atmosenv.2009.01.016.
41. Zhang K. et al., Integrated impacts of turbulent mixing and NOX-O3 photochemistry on reactive pollutant dispersion and intake fraction in shallow and deep street canyons, Sci. Total Environ. 712 (Apr. 2020) 135553, https://doi.org/ 10.1016/j.scitotenv.2019.135553.
42. Zhang S., Chen Y., Li Y., Yi X., Wu J. Study on Air Quality and Its Annual Fluctuation in China Based on Cluster Analysis. Int. J. Environ. Res. Public Health 2022, 19, 4524.
43. Zhang Y., et al., Numerical investigations of reactive pollutant dispersion and personal exposure in 3D urban-like models, Build. Environ. 169 (November 2019) (2020 a) 106569, https://doi.org/10.1016/j.buildenv.2019.106569.
44. Zhang Y., et al., Numerical studies of passive and reactive pollutant dispersion in high-density urban models with various building densities and height variations, Build. Environ. 177 (Jun. 2020 b) 106916, https://doi.org/10.1016/j. buildenv.2020.106916.
45. Zhong J., Cai X.-M.,. Bloss W.J. Large eddy simulation of reactive pollutants in a deep urban street canyon: coupling dynamics with O3-NO -VOC chemistry, Environ. Pollut. 224 (May 2017) 171–184, https://doi.org/10.1016/j.envpol.2017.01.076.

46. Zhou X. et al. Large eddy simulation of the effect of unstable thermal stratification on airflow and pollutant dispersion around a rectangular building, J. Wind Eng. Ind. Aerod. 211 (Apr. 2021) 104526, https://doi.org/10.1016/j.jweia.2021.104526.
47. Алоян А.Е. Динамика и кинетика газовых примесей и аэрозолей в атмосфере. Курс лекций. М.: ИВМ РАН, 2002.
48. Антонова А.М., Воробьев А.В., Воробьев В.А., Дутова Е.М., Покровский В.Д.. Моделирование распространения в атмосфере загрязняющих веществ выбросов электростанций на базе программного комплекса «SKAT». Известия Томского политехнического университета. Инжиниринг георесурсов. 2019. Т. 330. No 6. 174–18.
49. Атмосфера. Справочник (справочные данные, модели) // Ленинград: Гидрометеоиздат. 1991. 509 с.
50. Борисенко О. Н., Кузьменко М. В., Черенкова М. В., Гиниятуллина А. Г., Чухманов Н. В., Смолкина Д. Н., Тимаева Т. Е., Блажнова К. А. Вопросы атомной науки и техники. Сер. Математическое моделирование физических процессов 2022. Вып.3. С. 73-85.
51. Борисенко О. Н., Смолкина Д. Н., Черенкова М. В., Гиниятуллина А. Г., Кузьменко М. В., Чухманов Н. В., Потехина Е. В., Попова Н. В., Турусов М. Р. Вопросы атомной науки и техники. Сер. Математическое моделирование физических процессов 2018. Вып.2. С. 25-39.
52. Волков К.Н., Дерюгин Ю.Н., Емельянов В.Н., Козелков А.С., Тетерина И.В. Алгебраический многосеточный метод в задачах вычислительной физики // Вычислительные методы и программирование, т. 15, стр. 183-200, 2014.
53. Данилкин Е. А. , Лещинский Д. В. , Старченко А. В. . Микромасштабная математическая модель неизотермического турбулентного течения и переноса пассивной газообразной примеси в уличном каньоне. Вестник Томск. гос. ун-та. Матем. и мех., 2023, № 85, 117–131.
54. Данилкин Е.А., Старченко А.В. Моделирование распространения выбросов автомобильного транспорта в уличном каньоне. Вычислительные технологии. 2020. 25(2):4–21.
55. Ландау Л.Д., Лифшиц В.М., Гидродинамика // М.: Наука, 1988.
56. Лойцянский Л.Г. Механика жидкости и газа // М.: Наука, 1973.
57. Седляров О. И., Бородина Е. С. Моделирование распространения загрязняющих веществ в приземном слое атмосферы с учетом влияния застройки и рельефа местности // Промышленные процессы и технологии. 2022. Т. 2. № 2(4). С. 8–25. DOI: 10.37816/2713-0789-2022-2-2(4)-8-25

58. Старченко А.В., Данилкин Е. А., Лещинский Д. В. Численное моделирование распространения выбросов автотранспорта в уличном каньоне, Матем. моделирование, 2022, том 34, номер 10, 81–94.
59. Сухинов А. И. , Хачунц Д. С. , Чистяков А. Е. “Математическая модель распространения примеси в приземном слое атмосферы прибрежной зоны и ее программная реализация”, Ж. вычисл. матем. и матем. физ., 55:7 (2015), 1238–1254.
60. Сухинов А.И., Чистяков А.Е., Хачунц Д.С. Математическое моделирование движения многокомпонент- ной воздушной среды и транспорта загрязняющих веществ // Изв. ЮФУ. Техн. науки. 2011. № 8 (121). С. 73–79.